A POROSITY TECHNIQUE FOR THE DEFINITION OF OBSTACLES IN RECTANGULAR CELL MESHES

C. W. Hirt and J. M. Sicilian

Flow Science, Inc.
Los Alamos, New Mexico
August 1985

Abstract

Boundary fitted coordinates or adaptive mesh schemes have obvious advantages for the numerical solution of ship hydrodynamics problems. They also introduce a variety of numerical difficulties. For example, special generators must be devised to construct suitable meshes that fit the desired boundaries while maintaining convex cells with reasonable aspect ratios. Sometimes numerical stability requirements impose unacceptable time-step limits because of a few mesh cells with exceptionally small sizes. Numerical algorithms based on these methods also tend to be more complicated because of the added complexity associated with the changing shapes and orientations of the mesh cells.

In this paper we describe an alternative technique for computing flows bounded by complicated geometric shapes. Grid distortion problems are eliminated by using a grid composed of rectangular cells. Geometric boundaries are defined within this grid using a porosity technique in which the porosity has a zero value within obstacles and a unit value elsewhere.

Certain consistency requirements are presented that guide the porosity formulation into a numerical solution algorithm that has good stability properties. The resulting formulation can be used with the full Navier-Stokes equations or for potential flow applications. In either case, free surfaces of arbitrary deformation may be included using the Volume-of-Fluid (VOF) technique.

I. Introduction

A problem frequently confronting numerical analysts is how to represent complex geometric boundaries. For instance, in many fluid flow problems the flow region is bounded by curved walls, or variously-shaped obstacles may be embedded within the flow. In such cases the modeler is often driven to complicated finite-element methods or to simplified approximations, such as replacing curves by stair-step surfaces.

Although finite-element methods have achieved considerable success in many applications, their geometric flexibility is achieved at the expense of more complicated numerical algorithms. Furthermore, these methods may be subject to numerical accuracy and stability problems when the shapes and sizes of the elements vary rapidly from one element to the next.

Low order finite-element and finite-difference methods based on meshes of rectangular cells are logically simpler, easier to program, and easier to analyze for their stability and accuracy properties.

It is natural, therefore, to seek ways to model curved boundaries in these schemes.

A number of noteworthy attempts have been made to model curved boundaries in codes designed for incompressible fluid flow analysis. Viecelli [1] used a marker particle technique to represent arbitrary boundaries in a Marker-and-Cell type code. His scheme, which involved a pressure adjustment to prevent flow crossing a boundary, was quite successful for a variety of free surface flow calculations [2]. Hirt, et al [3] and McMaster and Gong [4] have used a somewhat simpler scheme in which selected velocities are adjusted in cells to satisfy a zero normal velocity boundary condition. When free surfaces are present, however, this method can lead to an over specification of the boundary conditions. This method also introduces some difficulties with regard to fictitious fluxes of mass and momentum across boundaries unless precautions are taken to specify values for flow variables outside the boundary.

Another possibility for modeling curved boundaries in rectangular grids is through the use of a variable porosity formulation. This concept is the subject of the present paper. True porous media flow models have existed for a long time. Usually a porous flow is dominated by viscous stresses arising from numerous tiny flow paths with a large surface-to-volume ratio. More recently the concept of a variable porosity has been used as a means of representing flow regions containing distributed obstructions that are too small to be resolved by the cells in a discrete grid. For example, codes used to model coolant flow in nuclear reactor cores [5,6,7] have employed this concept as a means of representing the fractional flow volumes and areas surrounding bundles of fuel rods and other structures.

The idea we wish to explore here is the use of a porosity that changes abruptly from unity to zero across a rigid boundary. The usual fluid dynamic equations are to hold in the region where the porosity is unity. Regions with zero porosity, that is, with zero flow volume are obstacle regions. Although this is a simple idea, it does not appear to have been previously explored as a general procedure.

In the next section we describe the porosity concept in more detail and derive the modifications needed in the fluid dynamic equations to include variable porosity effects. For simplicity, this discussion will be limited to two-dimensional, inviscid and incompressible flow, but the basic ideas can easily be extended to compressible, viscous and three-dimensional situations. In fact, some three-dimensional examples will be used as illustrations. The primary contribution of this paper is contained in Section III, which describes the special considerations needed to numerically approximate equations containing a discontinuous porosity. The numerical representation of a variable porosity is most conveniently defined in terms of fractional areas and volumes open to flow. Thus, the method described in this paper is referred to as the Fractional Area/Volume Obstacle Representation (FAVOR) Method. Section IV contains a discussion of such matters as numerical stability, accuracy and the relationship of the FAVOR method with other methods for representing obstacle boundaries. The question of accuracy will require a digression into the accuracy of nonuniform rectangular grids in general. This is done in Section IV.A, where it will be shown that approximations of conservation laws must lose some formal accuracy in variable grids. Examples illustrating the use of this new technique are presented in Section V.

II. Formulation of Equations

Equations describing fluid flow in a region containing multiple obstacles can be conveniently derived using the mathematical concept of generalized functions. This will be outlined in the next section. Then a brief discussion will be given of the methods used to reduce these equations to approximations on discrete grids. As might be expected, there are several steps in this reduction where, depending on the assumptions made, different approximating equations may be produced. Some attention will be given to the most important of these steps and justifications will be presented for the selections made.

A. Porous-Media Equations

To derive the equations for porous media we make use of the theory of generalized functions [8]. With this approach, boundary conditions at fluid-obstacle interfaces are automatically isolated in a convenient way. Let us consider by way of illustration the density equation,

$$\partial\rho/\partial t + \nabla\cdot\rho\underline{u} = 0 \qquad (1)$$

where ρ is the density and $\underline{u}$ is the fluid velocity. The density equation holds at all points occupied by fluid. A generalized (Heaviside) function of the spatial coordinate vector $\underline{x}$ and denoted by $H(\underline{x})$ is defined such that

$$H(\underline{x}) = \begin{cases} 1.0, & \text{if } \underline{x} \text{ is in the fluid} \\ 0.0, & \text{if } \underline{x} \text{ is in an obstacle.} \end{cases} \qquad (2)$$

If we now multiply the density equation by the step function H, the resulting equation can be considered as defined at all points in space. It agrees with the original equation, Eq. (1), in the fluid and is identically zero at points located in obstacles. The density function can be analytically continued into the obstacles in any manner for, as we shall see, its value in these regions will not be important.

The next step is to move the H function inside the time and spatial derivatives. To carry out the transposition, we shall need to evaluate derivatives of the step function H. Fortunately, it is known that the gradient of a step function is another generalized function - the delta function,

$$\nabla H(\underline{x}) = -2H\underline{n}\delta(\underline{x}-\underline{x}_s) \qquad (3)$$

where $\underline{x}_s$ is any point on the interface (surface) between the fluid and an obstacle. The vector $\underline{n}$ is a unit normal to the interface at location $\underline{x}_s$ and is directed out of the fluid. A formal derivation of Eq. (3) can be made using the techniques in Ref. [8], but we can see that it is intuitively correct from the following argument. Derivatives of H away from an interface are zero because H is then a constant function. For the same reason, a derivative of H parallel to an interface must also be zero. Gradients normal to an interface are infinite when evaluated at the interface because there H undergoes a step change. On the other hand, integration of a normal derivative of H across an interface gives a result of unity according to its definition. These properties are just those of a delta function, and this suggests the form of Eq. (3). The factor of 2H on the right side of the equation is introduced for convenience, but since H is discontinuous where the delta function is nonzero, a prescription is needed for evaluating the integral of such a product. The rule is

$$\int_{-1}^{+1} Q(z)\delta(z)dz = (Q_+ + Q_-)/2 \qquad (4)$$

where subscripts refer to values of Q on either side of z=0. Using this rule it is easy to see that the factor of 2H in Eq. (3) is consistent because an integration of that equation across $\underline{x}_S$ does produce an identity.

If the fluid-obstacle interfaces are time dependent, then we will also need the time derivative of H. This time dependency can only arise from a shifting of the boundary points with time. The time rate of change of boundary point $\underline{x}_S$ is just the velocity of the boundary $\underline{v}_S$, i.e.,

$$(d\underline{x}_S/dt) = \underline{v}_S \qquad (5)$$

Therefore, using the chain rule for differentiation the necessary time derivative is,

$$\partial H/\partial t = -(d\underline{x}_S/dt)\nabla\cdot H$$

$$= 2H\underline{v}_S\cdot\underline{n}\delta(\underline{x}-\underline{x}_S) \qquad (6)$$

Now, using Eq. (2) and Eq. (6) the density equation multiplied by H can be rewritten as

$$(\partial\rho H/\partial t) + \nabla\cdot(\rho H\underline{u})$$

$$+ 2\rho H(\underline{u}-\underline{v}_S)\,\underline{n}\delta(\underline{x}-\underline{x}_S) = 0 \qquad (7)$$

The last term involving the delta function is identically zero. To see this, first note that it is zero everywhere except at a fluid-obstacle boundary. At such a boundary it only has meaning when it is integrated across the boundary, but the integral is proportional to $(\underline{u}-\underline{v}_S)\cdot\underline{n}$ which is zero because the fluid velocity normal to an obstacle boundary must equal the normal velocity of the boundary.

A similar derivation can be used to derive the corresponding inviscid momentum equations in a porous medium, so that the final equations have the form

$$(\partial\rho H/\partial t) + \nabla\cdot(\rho H\underline{u}) = 0 \qquad (8a)$$

$$(\partial\rho H\underline{u}/\partial t) + \nabla\cdot(\rho H\underline{u}\underline{u}) = -H\nabla p + H\underline{g}\rho \qquad (8b)$$

where p is the fluid pressure and $\underline{g}$ is a body acceleration (e.g., gravity).

This is a special form of the porous-media equations in which the porosity is a discontinuous function. That is, the porosity is either 0.0 or 1.0. To apply this result to a material like sand where the positions of individual sand grains are unknown, it is first necessary to perform an ensemble average on Eqs. (8). Only H varies in the ensemble average because it depends implicitly on the arrangement of the obstacles (i.e., the sand grains). Therefore, after averaging we replace H in Eqs. (8) with its ensemble average, say f. The quantity $f(\underline{x})$ is the average porosity (or it may be equivalently interpreted as the probability that an obstacle does not exist at location $\underline{x}$). For our purposes we wish to keep Eqs. (8) as they are so that we may use H to describe well-defined arrays of obstacles.

B. Coarse-Scale Approximations

Let us integrate the density equation over a small volume in space, R, with boundary surface S. Within R there will, in general, be subregions containing fluid and subregions containing obstacles. The interfaces between these regions within R will be denoted by I. The average of the density equation over region R is

$$\frac{1}{R}\int_R \left(\frac{\partial\rho H}{\partial t} + \nabla\cdot\rho H\underline{u}\right)dR = 0 \qquad (9)$$

where R is here used for both the volume of the region and as an indicator for the limits of

integration. Since R is independent of time, the leading term in Eq. (9) is

$$\frac{1}{R}\int_R \frac{\partial}{\partial t}(\rho H)dR = \frac{\partial}{\partial t}\left(\frac{1}{R}\int_R \rho H dR\right) \quad (10)$$

In making finite-volume approximations for numerical solution algorithms, the region R would be one element or cell of a grid that divides the flow region into a set of control volumes. For a useful approximation, the grid cells must be chosen small enough so that within a cell the dependent variables describing the flow can be treated as constants (or possibly as having some simple spatial variation). Neglecting flow variations over scales covered by region R compared to variations over the entire region of interest is called the coarse-scale approximation. When this assumption is satisfied, the density in the volume integration in Eq. (10) can be replaced by its mean value so that

$$\frac{1}{R}\int_R \rho H dR = \rho V \quad (11)$$

where

$$V = \frac{1}{R}\int_R H dR \quad (12)$$

The quantity V is defined, for arbitrary R, as the fractional volume open to flow.

A similar result can be obtained for the divergence term in Eq. (9). First, Gauss' divergence theorem is used to reduce the volume integration to a surface integral.

$$\frac{1}{R}\int_R \nabla\cdot\rho H\underline{u}dR = \frac{1}{R}\int_S \rho\underline{u}\cdot\underline{n}HdS \quad (13)$$

The integral is the flux of fluid out of region R through the open portion of its boundary S. Usually the boundary is subdivided into a set of segments S such that the coarse-scale approximation can be applied to each segment. For example, for segment i,

$$\frac{1}{S_i}\int_{S_i} \rho\underline{u}\cdot\underline{n}HdS_i = \rho\underline{u}\cdot\underline{n}_i A \quad (14)$$

where

$$A = \frac{1}{S_i}\int_{S_i} H dS_i \quad (15)$$

The quantity A is defined, for arbitrary S_i, as the fractional area open for flow across surface S_i.

If the functions V and A are continuous and differentiable, it can be shown that they must be equal to the same function. However, our goal is the derivation of finite-volume equations in which these quantities may be discontinuous functions. Thus, we see that several fractional volumes and areas must be associated with each control volume.

C. Pressure Gradient Averages

Consider the volume averaging process applied to the pressure gradient term appearing in Eq. (8b),

$$\frac{1}{R}\int_R HV p dR \ . \quad (16)$$

An alternative form is

$$\frac{1}{R}\int_R (\nabla(pH) - p\nabla H)dR$$

$$= \frac{1}{R}\int_R (\nabla(pH) + 2Hp\underline{n}\delta(\underline{x}-\underline{x}_s))dR \quad (17)$$

$$= \frac{1}{R}\int_S pH\underline{n}dS + \frac{1}{R}\int_I p\underline{n}dI$$

where the last integral has been reduced using Eq. (4) and I indicates

integration over all fluid-obstacle interfaces located within R. This alternative form is easy to interpret; the first integral is the pressure force acting on the fluid along the open portion of the surface S that surrounds R, the second integral is the pressure force acting on the fluid at all interior fluid-obstacle interfaces.

The question is, which of these forms, Eq. (16) or Eq. (17), is best suited for finite-volume approximations? When the pressure is nearly constant within R, both expressions are approximately zero and neither one is preferable over the other. However, when there is a hydrostatic equilibrium, the pressure gradient is constant and the expression in Eq. (16) reduces immediately to $V\nabla p$.

When there is a hydrostatic equilibrium, the second term on the right side of Eq. (17) is equal to the net buoyant force experienced by the obstacles within R and cannot be ignored. In any case, neither term on the right side of Eq. (17) can be easily approximated in this limit. Some authors have used the coarse-scale approximation $\nabla(pV)$ for the first term, but since the second term cannot be ignored, this is not a useful or convenient approximation. Thus, for a coarse-scale approximation it is best to assume the pressure gradient rather than the pressure is nearly constant.

In dynamic situations, when the pressure differs from hydrostatic, the approximation, $V\nabla p$, is not exact for it neglects non-viscous drag effects imposed on the fluid by the obstacles. If these drag forces are significant, it is necessary to add them separately to the approximation. When doing this, however, it must be remembered that buoyant forces on obstacles are not to be included in the addition.

III. Finite-Volume Equations

A mesh of nonuniform rectangular cells will be used as the basis for our finite-volume equations. Using a nonuniform mesh helps us identify some points regarding accuracy and also allows a comparison of the FAVOR method with more standard techniques. Some simplifications are in order, however, to keep the presentation manageable. Thus, the following development will be limited to the case of two-dimensional, incompressible fluid flow with constant density. The density equation, Eq. (8a), with the density divided out is referred to as the continuity equation. After dividing the momentum equations by ρ the ratio of pressure to constant density will again be denoted by p. Extensions to three-dimensional flows or to flows with variable density is straightforward.

Dependent variables are to be placed at staggered grid locations as illustrated in Fig. 1A. The staggered grid dates back to the Marker-and-Cell (MAC) method [9] and is particularly well suited for approximations based on the primitive variables, pressure and velocity.

A simplified subscript notation, Fig. 1B, will be used to indicate mesh locations relative to a generic cell center at (i,j). Location (i,j) will be denoted by the subscript C. In general, upper case letters N, S, E, and W denote shifts in the principal compass directions by one integer. For instance, E refers to location (i+1,j), while N refers to location (i,j+1). Similarly, the lower case letters n, s, e, and w will denote corresponding shifts of half integer values. Multiple integer shifts are represented by repeated letters. The order of the letters is unimportant. Some examples should make it clear how this convenient notation works.

$$u_{i,j} = u_C$$

$$u_{i+1/2,j} = u_e$$

$$u_{i+1/2,j+1/2} = u_{ne}$$

$$u_{i-3/2,j+2} = u_{NNWw}$$

$$\delta x_i = \delta x_C$$

Using finite-volume and time averages, the density and momentum equations can be reduced to discrete (difference) equations. This formal reduction, however, involves a variety of integrated quantities at different mesh locations. These quantities must be treated as independent unless limit properties or consistency arguments can be found to eliminate them as unknowns. For instance, we will find that consistency requires certain quantities at one mesh location to be simple combinations of similar quantities at neighboring locations.

We begin by averaging the continuity equation over a generic mesh cell (i,j) and over the time interval from t to t+δt,

$$(V^{n+1}-V^n)/\delta t + (\langle Hu\rangle_e-\langle Hu\rangle_w)/\delta x_C + (\langle Hv\rangle_n-\langle Hv\rangle_s)/\delta y_C = 0 \qquad (18)$$

where V is the volume integral defined in Eq. (12) and angled brackets indicate the time and surface averages defined as

$$\langle Q\rangle = \frac{1}{\delta t}\int dt \frac{1}{S}\int_S Q dS \ . \qquad (19)$$

Strictly speaking, there are two different angled-bracket averages appearing in Eq. (18): those containing a u-velocity are integrated with respect to the y-direction, while those containing v-velocities are integrated with respect to the x-direction. This will not cause confusion since we are considering each quantity with a different argument or at a different location as an independent quantity.

The momentum equation for the u-velocity located at mesh position e is to be averaged in space over a rectangle that extends from location C to location E, see Fig. 2. Integrating over this region and over time interval δt we have

$$(\overline{Hu}^{n+1} - \overline{Hu}^n)/\delta t + (\langle Huu\rangle_E - \langle Huu\rangle_C)/\delta x_e + (\langle Hvu\rangle_{ne} - \langle Hvu\rangle_{se})/\delta y_C = -V_e(p_E-p_C)/\delta x_e + V_e g_x \qquad (20)$$

where Guass' theorem has been used to reduce the divergence term to surface integrals, and where $\delta x_e = (\delta x_C + \delta x_E)/2$. The overbar indicates a volume average similar to that in Eq. (12). For the pressure terms, we have used the coarse-scale approximation described earlier, in which the pressure gradients are roughly constant in time.

The averaged equations, Eqs. (18) and (20), involve many undefined quantities. To proceed further we must either introduce ad hoc approximations or seek some additional equations that will reduce the number of unknowns. One possibility is to look for consistency relationships. For instance, in the original differential equations, Eqs. (8), the density equation can be subtracted from the momentum equation to give an equation for just the velocity, i.e.,

$$(\partial \underline{u}/\partial t) + \underline{u}\cdot\nabla\underline{u} = -\nabla p + \underline{g} \qquad (21)$$

This type of equation manipulation is essential for deriving shock wave jump conditions in compressible flow, Bernoulli's equation and many other

useful relationships. It is reasonable, therefore, to require our discretized equations to have the same property. The goal is to separate the discretized continuity equation, Eq. (18), from Eq. (20) so that the resulting equation will be a discrete approximation to Eq. (21). It is immediately obvious that this cannot be done unless the bar-average of the product Hu appearing in the time-derivative term in Eq. (20) is separable into a product of bar-averages. Similarly, the angled-bracket averages, which involve a product of two velocities, must be separable into a product of averages in which one factor is of the form appearing in Eq. (18). Thus, for consistency with the equation separation process, we must first require relations of the form

$$\begin{aligned} \overline{Hu}_e &= V_e u_e \\ \langle Huu\rangle_C &= \langle Hu\rangle_C u_C^* \\ \langle Hvu\rangle_{ne} &= \langle Hv\rangle_{ne} u_{ne}^* \end{aligned} \qquad (22)$$

The u_e in the first relation is centered at the cell edge where we started the averaging process so no special notation is used to mark this quantity. The u* velocities appearing in the second two relations are located at cell positions other than the primary, staggered mesh positions so these quantities have the superscript *. We shall interpret these relations as definitions for these new quantities. That is, relations (22) are needed for their form, but no approximations have been made if we consider them as definitions.

Using these definitions, the time derivative term in Eq. (20) can be rewritten in the form

$$[(V_e^{n+1}-V_e^n)u_e^n+V_e^{n+1}(u_e^{n+1}-u_e^n)]/\delta t \qquad (23)$$

Again using the definitions, Eq. (22), and adding and subtracting inside the parentheses, terms equal to the u_e times each of the angled bracket terms, we can rearrange Eq. (20) to

$$\begin{aligned} &V_e^{n+1}(u_e^{n+1}-u_e^n)/\delta t \\ &+[\langle Hu\rangle_E(u_E^*-u_e)+\langle Hu\rangle_C(u_e-u_C^*)]/\delta x_e \\ &+[\langle Hv\rangle_{ne}(u_{ne}^*-u_e)+\langle Hv\rangle_{se}(u_e-u_{se}^*)]/\delta y_C \\ &= -V_e(p_E-p_C)/\delta x_e+V_e g_x - D_e u_e^n \end{aligned} \qquad (24)$$

where D_e is given by the expression,

$$\begin{aligned} D_e = {} & (V_e^{n+1}-V_e^n)/\delta t+(\langle Hu\rangle_E-\langle Hu\rangle_C)/\delta x_e \\ & + (\langle Hv\rangle_{ne}-\langle Hv\rangle_{se})/\delta y_C \end{aligned} \qquad (25)$$

Equation (24) is almost the discretized version of Eq. (21), except that it has the extra term containing D_e. However, D_e looks like the left side of the discrete continuity equation, Eq. (18), evaluated at the cell edge location e and not at a cell center as is Eq. (18). To complete the equation separation we note that D_e could be rewritten as

$$D_e = (\delta x_E D_E+\delta x_C D_C)/(\delta x_E+\delta x_C) \ , \qquad (26)$$

where the D's on the right side are now cell-centered expressions, if we make the following correspondences

$$\begin{aligned} \langle Hu\rangle_C &= (\langle Hu\rangle_e+\langle Hu\rangle_w)/2 \\ \langle Hv\rangle_{ne} &= (\delta x_C\langle Hv\rangle_n \\ &\quad +\delta x_E\langle Hv\rangle_{nE})/(\delta x_C+\delta x_E) \\ V_e &= (\delta x_C V_C+\delta x_E V_E)/(\delta x_C+\delta x_E) \end{aligned} \qquad (27)$$

These relations express the way

quantities at intermediate mesh locations are related to similar quantities at their primary locations. Using them, the D_e term appearing in Eq. (24) is identically zero when Eq. (18) is satisfied and we have completed the desired equation separation.

If we do a similar reduction on the v-momentum equation, then combine all assumptions and consistency requirements, the momentum equations can now be written as,

$$(u_e^{n+1}-u_e^n)/\delta t + (f_{xE}Q_E+f_{xC}Q_C+f_{xn}Q_n+f_{xs}Q_s)/V_e^{n+1} = -(p_E-p_C)/\delta x_e+g_x \qquad (28a)$$

$$(v_n^{n+1}-v_n^n)/\delta t + (f_{ye}R_e+f_{yw}R_w+f_{yN}R_N+f_{yC}R_C)/V_n^{n+1} = -(p_N-p_C)/\delta y_n+g_y \qquad (28b)$$

where

$$Q_E = 2\langle Hu\rangle_E(u_E^*-u_e^n)/\delta x_E\ , \qquad f_{xE} = \delta x_E/(\delta x_C+\delta x_E)$$

$$Q_C = 2\langle Hu\rangle_C(u_e^n-u_C^*)/\delta x_C\ , \qquad f_{xC} = \delta x_C/(\delta x_C+\delta x_E)$$

$$Q_n = 2\langle Hv\rangle_{ne}(u_{ne}^*-u_e^n)/\delta y_C\ , \qquad f_{xn} = 1/2$$

$$Q_s = 2\langle Hv\rangle_{se}(u_e^n-u_{se}^*)/\delta y_C\ , \qquad f_{xs} = 1/2 \qquad (29)$$

$$R_e = 2\langle Hu\rangle_{ne}(v_{ne}^*-v_n^n)/\delta x_C\ , \qquad f_{ye} = 1/2$$

$$R_w = 2\langle Hu\rangle_{nw}(v_n^*-v_{nw}^n)/\delta x_C\ , \qquad f_{yw} = 1/2$$

$$R_N = 2\langle Hv\rangle_N(v_N^*-v_n^n)/\delta y_N\ , \qquad f_{yN} = \delta y_N/(\delta y_C+\delta y_N)$$

$$R_C = 2\langle Hv\rangle_C(v_n^n-v_C^*)/\delta y_C\ , \qquad f_{yC} = \delta y_C/(\delta y_C+\delta y_N)$$

On the right side of Eq. (28a) we have dropped the factor V_e/V_e^{n+1} because we could just as well have used V_e^{n+1} on the right side of Eq. (24). A similar factor has been dropped from Eq. (28b). Equation (28a) has the desired form of Eq. (21) because the Q_E and Q_C terms defined in Eq. (29) are approximations for $Hu(\partial u/\partial x)$ while Q_n and Q_s are approximations of $Hv(\partial u/\partial y)$. The f factors are weighting factors dependent on the cell sizes. In a uniform grid the f's are all equal to one half.

To summarize, relations (27), which were used to give the discretized equations the same separation property as the differential equations, have reduced the number of unknowns in the discretized equations. Unfortunately, there are still more unknowns than equations. The remaining unknowns are,

$$u_e\ ,\ v_n\ ,\ p_C$$
$$u_C^*\ ,\ u_{ne}^*\ ,\ \langle Hu\rangle_e \qquad (30)$$
$$v_C^*\ ,\ v_{ne}^*\ ,\ \langle Hv\rangle_n$$

Quantities u_e, v_n, and p_C are the primary variables at the staggered mesh locations we designated at the outset. All remaining quantities are secondary unknowns that must still be specified.

A course-scale approximation could be used to separate out the H-function from the two unknowns in which it appears.

$$\langle Hu\rangle_e = A_e u_e^* \qquad \langle Hv\rangle_n = A_n v_n^* \tag{31}$$

where A_e and A_n are the fractional areas open to flow at the sides of a mesh cell and two new velocity averages have been introduced. Now all the secondary unknowns (indicated by a superscript *) have a similar form: i.e., they are all related to surface-time averages of velocities.

Up to this point the equations derived are essentially "exact" in that we have only made substitutions in terms of new unknowns, but to proceed further we must now introduce approximations that relate these unknowns to the primary dependent variables. First, it should be noted that no time levels have been assigned to the various fluxing velocities. If time level n+1 values are used, the resulting equations are implicit and would require a complicated procedure for their simultaneous solution. Using only time level n values results in explicit equations that are easy to solve, but it is well known that these equations may be numerically unstable unless the approximations are carefully chosen [10]. Before deciding on suitable approximations, it will be worthwhile to first look into questions of accuracy and stability.

IV. Other Matters

A. Accuracy in a Nonuniform Mesh

The horizontal advection of momentum in Eq. (28a) is contained in the sum $f_{xE}Q_E + f_{xC}Q_C$. Accuracy refers to how rapidly this finite-volume expression approaches the limiting differential for $Hu(\partial u/\partial x)$ at location e as δt and the volume of the cell are reduced to infinitesimal values. If the difference between the finite-volume and limiting forms is proportional to the N-th power of δt and M-th power of the cell size, the accuracy is said to be N-th order in time and M-th order in space.

A typical approximation is to identify the u^* velocity in Eq. (31) with the u velocity defined in Eq. (22). In other words, equate surface and volume averaged quantities at the same location. If in Q_E we then set u_E^* equal to an average of the neighboring boundary centered velocities,

$$u_E^* = (u_e^n + u_{eE}^n)/2 \tag{32}$$

this corresponds to a centered difference approximation. Q_E is then a second order (in space) approximation to $Hu(\partial u/\partial x)$ at location E. A similar centered approximation in Q_C makes it a second order approximation at location C. Unfortunately, the combination of the two Q's is only first order accurate at location e because in a nonuniform mesh the f-weighting factors do not have the correct values. A correct second order approximation at e requires the interpolated expression $f_{xC}Q_E + f_{xE}Q_C$, while the expression $f_{xC}Q_C + f_{xE}Q_E$ is second order only at the midpoint between locations C and E. Since this point does not correspond to location e (unless the mesh is uniform), Eq. (28a) cannot be more than first order accurate at position e.

If a donor cell or upstream approximation is used for the u_E^* velocity, then the situation is worse. For instance, if the velocity is positive, then Q_E is zero and $f_{xC}Q_C$ becomes a second order approximation at location C, but at e the approximation is zeroth order accurate because the first term in a Taylor series expansion about e will have the extra coefficient $2f_{xC}$. In a mesh

with slowly varying cell sizes $2f_{xC}$ can be significantly different from unity. For example, a 20% change in neighboring cell sizes produces a 10% error in the coefficient.

Now consider the vertical advection terms in Eq. (28a). Regardless of whether a centered or donor cell assumption is used for the u^* velocities, the Q_n and Q_s terms are zeroth order accurate approximations for $Hv(\partial u/\partial y)$, because only δy_C appears in these expressions. That is, first or higher order derivative approximations require the appearance of δy_N and δy_S values if the mesh is nonuniform. A special choice for the Q's does exist, however, that will produce a first order approximation for these terms.

We conclude, therefore, that consistent finite-volume equations based on a staggered mesh are formally first-order accurate in a nonuniform mesh. A first-order approximation can be achieved using the donor cell approximation only if we give up the rigorous conservation form of the equations, for example, by modifying the f-weighting factors. A simple choice for these factors that produces a first order approximation is,

$$f_{xE}=f_{xC}=1/2$$

$$f_{xn}=\delta y_C/(\delta y_C+\delta y_N) \quad , f_{xs}=\delta y_C/(\delta y_C+\delta y_S)$$

$$f_{ye}=\delta x_C/(\delta x_C+\delta x_E) \quad , f_{yw}=\delta x_C/(\delta x_C+\delta x_W)$$

$$f_{yN}=f_{yC}=1/2 \qquad (33)$$

If we do not permit approximations that use values separated by more than one δx or one δy, the approximations can never be more than first order accurate.

B. Stability Considerations

It is important to consider what numerical stability requirements must be imposed on the FAVOR method. This is particularly necessary if the fractional volume of a cell is allowed to approach zero, which may occasionally happen when a curved boundary is embedded in a mesh.

A rigorous analytical treatment of stability is not possible because the coefficients of the advection terms are not constant. However, we can make a heuristic assessment based on effective advection speeds. In the case of a uniform mesh with unit area/volume fractions the usual stability conditions for an explicit approximation are that fluid must not move across more than one cell in one time step. In two dimensions this condition is usually replaced by the restriction that fluid not move more than one fourth of the cell width so that the maximum possible volume fluxed out of the four sides of the cell will not exceed the volume of the cell.

Referring to Eqs. (28), (29), and (31) we note that in the FAVOR method the advection velocities are multiplied by the ratio of a fractional side area to a fractional volume. These modified velocities must still conform with the requirement that the maximum volume fluxed out of a cell not exceed the cell volume. Therefore, to see how stability is influenced by FAVOR we must investigate the values of area to volume ratios appearing in the finite-volume equations. Only two limiting cases need to be considered. For a typical u velocity, say u_e, suppose cell C to its left is almost closed off (i.e., V_C is almost zero). This closure may be due to an obstacle surface oriented either vertically or horizontally, see Fig. 3A. In the vertical case A_e and V_E will be unity, and A_n and V_N will be equal to V_C. Because the fractional volume V_e appearing in the u-velocity equation is a weighted average of V_C and V_E, Eq. (27), it can be shown that the maximum area to volume ratio appearing Eq. (28a) is $A_e/V_e = (\delta x_C + \delta x_E)/\delta x_E$, which is equal to 2.0 in a

uniform mesh. A factor of two increase in the effective advection velocities causes no serious problems for stability.

The second case to consider is a horizontal surface that is tending to close off cell C and cell E, see Fig. 3B. In this instance V_e is tending to zero (with both V_C and V_E) and the worst case is associated with vertical advection through the fully open top cell faces. It appears that the vertical flux $A_n v_n / V_e$ is tending to infinity as V_e tends to zero. However, v_n is simultaneously tending to zero in this case because the continuity equation requires $A_n v_n \delta x_C$ to be proportional to $A_e u_e \delta y_C$, and the vertical flux is then proportional to $u_e \delta y_C / \delta x_C$. Therefore, the vertical advective flux is actually bounded and stability of the momentum equations is again easily maintained.

These simple considerations show that the FAVOR method, as formulated in this paper, should have no serious stability problems, even when mesh cells are closed off to a tiny fraction of their original size. This expectation has been verified in numerous calculations and will be demonstrated in Section V.

C. Relationship between FAVOR and Other Obstacle Methods

When the area and volume fractions are all set to unity, The FAVOR scheme reduces to a standard type of nonuniform mesh approximation. Using this observation, we can see how FAVOR is related to other obstacle representations. Suppose we wish to model the presence of a rigid, vertical wall in a grid of equal-sized cells, but the wall does not coincide with a grid line. The standard procedure would be to introduce one cell of smaller size at the wall (i.e., a nonuniform mesh) so that the wall would then lie at a grid line, as shown in the top sketch of Fig. 4. Here the small cell has width h and the wall lies at its left boundary. In the FAVOR scheme we keep a uniform mesh, but define the wall's presence by assigning fractional areas and volumes to the cell containing the wall. This is indicated in the bottom sketch of Fig. 4, where the shaded area represents the region of zero porosity. Now, to evaluate the two approaches let us compare the difference equations that would be used in each case for the u_e velocity. In making this comparison it must be noted that $V_C \delta x$ is equal to h. The reader can easily carry out the details so we simply state that the two equations are identical except for the pressure gradient terms. In the FAVOR method the gradient is evaluated as a pressure difference over a distance δx, while in the nonuniform mesh it is evaluated as a difference over a distance $(\delta x + h)/2$. Also, the spatial locations of P_C and v_n are different in the two cases.

A similar comparison can be made for the v_n velocity. In this instance the two evaluations result in identical difference equations, including the pressure gradients. Furthermore, the continuity equation is the same in both cases.

Now we note that the difference in variable locations in the two approaches is less than one cell width, so these approximations differ by a term that is first order in space. The pressure gradient difference noted above is also of first order. Thus, FAVOR agrees to first order with a nonuniform mesh approximation, but since the latter can only be first order accurate we conclude that the FAVOR method does not reduce the accuracy of the approximations.

Other techniques for embedding curved or diagonal boundaries in a rectangular mesh [1,2,3,4] rely on first order spatial interpolation or extrapolation approximations. Therefore, FAVOR is also comparable in accuracy to these methods.

D. Boundary Conditions

The formulation of the FAVOR method would make it appear that no special considerations are needed at obstacle boundaries. Unfortunately, this is true only in the differential formulation, but not in the finite-volume approximations. A simple example will illustrate the problem. Figure 5A shows a two-dimensional duct with parallel walls oriented at an angle to the grid lines of a uniform mesh. Fractional cell areas and volumes are used to define the duct walls. Since the walls are not aligned with the cell diagonals, there is a wide range of fractional cell sizes. A uniform flow of incompressible fluid, directed from left to right, was initially defined in the duct as shown in Fig. 5B. This velocity was held constant at the left side of the mesh, while at the right side a constant pressure condition was maintained. Under these conditions the flow should remain constant and uniform. In Fig. 5C we see this is not the case. A parabolic-like profile has developed after the flow has moved approximately one duct length. The dashed and vertical lines were added to emphasize this velocity profile.

These poor results are caused by advective flux approximations that require a velocity component located inside an obstacle. In Fig. 5C we used zero values for these velocities and as a consequence an unrealistically low flux was computed that eventually produced the artificial boundary layer. To correct this defect a simple device is required; the difference expressions for all fluxes are formulated in terms of velocity derivatives. Then, all the derivatives at interfaces are set to zero. In this way all boundaries become free-slip boundaries. (When viscous shear stresses are wanted they can be added as separate force contributions.) A repeat calculation of the duct problem using this boundary treatment is shown in Fig. 5D. Here we see the flow now remains nicely uniform, even though the calculation was further complicated with a non-uniform mesh spacing in the horizontal direction.

The maximum velocity component computed in Fig. 5D is actually 1.5% larger than the initial horizontal velocity. This small discrepancy arises because there are a few cells where the fractional volume open for fluid is less than 1%. In the code we somewhat arbitrarily set any cell face area or cell volume that is less than 1% open to be a zero area or zero volume. Consequently, at these locations small perturbations modify the otherwise uniform flow. The 1% cutoff on fractional areas and volumes has been found to be a useful practical limit. This example is a good illustration of the stability of the FAVOR scheme when used with a wide range of fractional volumes.

V. Examples

All the examples described in this section were obtained using the HYDR-3D program [11]. This program is a general purpose analysis tool for compressible or incompressible flow that uses the FAVOR method to provide a general geometric modeling capability. For incompressible flows, the program uses the Volume of Fluid (VOF) technique to track free surfaces and two-fluid interfaces.

A. Potential Flow around a Cylinder

As a first demonstration of the usefulness of the Fractional Area/Volume Obstacle Representation method, we have computed the potential flow about an impulsively accelerated cylinder. More specifically, the Euler equations were solved for the impulsive acceleration of flow from rest to a uniform speed about a fixed cylinder. Since the velocity field generated in one time step is proportional to the gradient of a scalar (the pressure) and satisfies the continuity equation, the resulting

flow is potential flow. If the fluid starts from rest, the theoretical (inertial) drag coefficient [12] should be 2.0 which arises from the combined effect of an acceleration needed to set the fluid into motion and an acceleration needed to establish flow about the cylinder.

For this calculation the mesh used is illustrated in Fig. 6. The large mesh region minimizes influences from the boundaries, but the cylinder is only resolved by about 4 to 5 cells across its radius. A generator program, which was used to automatically set the fractional areas and volumes, produced a volume for the cylinder that was 0.5% smaller than the exact volume.

Figure 6B shows a portion of the computed potential velocity field in the immediate vicinity of the cylinder. The computed inertial drag coefficient based on the acceleration that set the flow into motion in one time step was 2.05, or 2.5% larger than the theoretical value. This is remarkably good considering that pressure forces on the coarsely defined cylinder were simply computed using cell-centered pressures times the adjacent cell face areas occupied by the obstacle.

B. Cylindrical Tank Slosh

To show the effectiveness of the FAVOR method for problems having free surfaces we have investigated the problem of fluid slosh in a right circular cylinder. For low amplitude sloshing there is an analytic theory with which to make comparisons. This is an ideal test case because the geometry can be modeled exactly using cylindrical coordinates or approximated with the fractional areas/volumes of the FAVOR technique in a Cartesian coordinate system. A third possibility is to use a Cartesian mesh with cells either fully open or fully blocked to produce a stepped-boundary that approximately defines the cylinder. These three cases are illustrated in Fig. 7. In the middle plot, the curved boundary actually used in the FAVOR calculation is not shown by the method used to plot the surface perspective.

The slosh problem consists of shaking the tank sinusoidally in a horizontal direction and measuring the fluid height at the side wall. Because of symmetry only one half of the tank needs to be modeled. Figure 8 shows a comparison of the first two methods in terms of the time histories of the computed fluid heights. There is no significant difference in the results obtained with the cylindrical mesh and with the Cartesian mesh using the FAVOR scheme. However, the cylindrical mesh calculation required about 10 times more computational time because the small cells near the central axis required a smaller time step to maintain stability. Thus, the FAVOR method is seen to work extremely well and, for this example, required an order of magnitude less CPU time.

The relatively poor performance of the third method, which used a stepped boundary approximation, is shown in Fig. 9. Finally, Fig. 10 shows that either of the first two results are in close agreement with linear theory [13]. (The time shift between the two curves in this plot is only about one computational time step.)

Total computational time on a CDC 7600 computer for 588 mesh cells and 172 time cycles was 2.87 min using the Cartesian mesh. (In the cylindrical mesh 798 cells were used and the time required for 677 time cycles was 31 min.).

C. Spherical Tank Slosh

A problem closely related to the above is slosh in a spherical tank when it is shaken horizontally. For the 50% filled case there is also a linear theory with which to make comparison [14]. Using FAVOR to define the spherical tank in a

rectangular, Cartesian grid, we produced the results shown in Fig. 11. Here the computed and theoretical fluid heights at the side wall are almost indistinguishable, which again confirms the effectiveness of the FAVOR method.

D. Wigley Model 1805A

To illustrate the use of the FAVOR method for ship-wave resistance problems, we calculated the flow about an impulsively started Wigley Model 1805A ship. This problem has previously been solved numerically by various researchers. Dawson [15] used this model as a test of his panel method, while Ohring and Telste [16] solved the transient problem using a finite-difference solution of the linearized potential flow equations.

Following Dawson, we define the body surface by

$$y = 0.75(1-z^2)(1-x^2/64)(1-0.6x^2/64), \tag{34}$$

and have used his recommended flow region (3/8L wide, 1/4L upstream and downstream of the body, and 3/16L deep, where L is the body length). Figure 12 shows a cross section of the mesh with the midship section drawn in (only one half of the problem is modeled because of symmetry). The mesh was chosen to roughly correspond to Dawson's resolution of 64 panels on the body and 224 panels on the free surface. In our case the mesh consisted of 24x12x10 = 2880 cells in the flow region. At time zero the flow was impulsively accelerated to a value corresponding to a Froude number of $u/\sqrt{gL} = 0.503$.

Figure 13 shows the computed flow resistance, $C_R = R/(\rho u^2 Ld)$, in comparison with the results of Ohring and Telste, where R is the computed force and d the draft. Except for a peculiar fluctuation observed around 0.75 body traversal times, the computed wave resistance goes almost monotonically to a steady value that is slightly below the experimentally observed value of 0.0044 (lower dashed line in Fig. 13). The fluctuation is probably a numerical artifact, but its exact origin has not been determined. A second calculation at a Froude number of 0.45, Fig. 13, did not exhibit this problem. In this case the computed wave resistance lies between the thin ship prediction and the experimentally observed value.

It is interesting that we do not see the oscillatory transients observed by Ohring and Telste. This may be due to the non-linear treatment and more exact body boundary conditions that we have used. It is known, for example, that nonlinear advection effects can have a smoothing influence on wave interactions. The wave profile computed along the body in the 0.503 Froude number case is shown in Fig. 14. Here the agreement along the stern half of the body is good, but along the bow half the wave heights are not as good as one would desire. In particular, the height of the bow wave is under predicted. This could have been a consequence of using the Wigley hull shape above the still water level (SWL). If the model tests used a straight-sided model above the SWL, one would expect to see a larger bow wave. Unfortunately, no information was available to us regarding the actual model geometry in this region.

References

1. Viecelli, J.A., "A Method for Including Arbitrary External Boundaries in the MAC Incompressible Fluid Computing Technique," J. Comp. Phys., 4, 543 (1969).

2. Viecelli, J.A., "A Computing Method for Incompressible Flows Bounded by Moving Walls," J. Comp. Phys. 8, 119 (1971).

3. Hirt, C.W., Nichols, B.D., and Romero, N.C., "SOLA-A Numerical Solution Algorithm for Transient Fluid Flows," Los Alamos Scientific Laboratory report LA-5852 and "Addendum," LA-5852, Add. (1975).

4. McMaster, W.H. and Gong, E. Y., "PELE-IC User's Manual," Lawrence Livermore Laboratory report UCRL-52609 (1979).

5. Stewart, C.W., et al, "COBRA-IV: The Model and the Method," Battelle Pacific Northwest Laboratories report BNWL-2214 (1977).

6. Domanus, H.M., et al, "COMMIX-1A: A Three-Dimensional Transient Single-Phase Computer Program for Thermal-Hydraulic Analysis of Single and Multicomponent Systems, Vol.I: User's Manual," NUREG/CR-2896 (1983).

7. "TRAC-PD2: An Advanced Best-Estimate Computer Program for Pressurized Water Reactor Loss-of-Coolant Accident Analysis," Los Alamos National Laboratory report LA-8709-MS and NUREG/CR-2054 (1981).

8. Lighthill, M.J., Introduction to Fourier Analysis and Generalized Functions, Cambridge Univ. Press (1958).

9. Harlow, F.H. and Welch, J.E., "Numerical Calculations of Time-Dependent, Viscous, Incompressible Flow," Phys. of Fluids, 8, 2182 (1965).

10. Hirt, C.W., "Heuristic Stability Theory for Finite-Difference Equations," J. Comp. Phys. 2, 339 (1968).

11. Sicilian, J.M. and Hirt, C.W., "HYDR-3D: A Solution Algorithm for Transient 3D Flow," Flow Science, Inc. report FSI-84-00-3 (1984).

12. Sarpkaya, T., "Separated Flow about Lifting Bodies and Impulsive Flow about Cylinders," AIAA Jour. 4, 414 (1966).

13. Hunt, B. and Priestley, N., "Seismic Water Waves in a Storage Tank," Bull. Seismological Soc. Am. 68, 487 (1978).

14. Budiansky, B. "Sloshing of Liquids in Circular Canals and Spherical Tanks," J. Aero/Space Sci., 27, No. 3 (1960).

15. Dawson, C.W., "A Practical Computer Method for Solving Ship-Wave Problems," Proc. Second International Conf. Num. Ship Hydro., UCB (1977).

16. Ohring, S. and Telste, J., "Numerical Solutions of Transient Three-Dimensional Ship-Wave Problems," Proc. Second International Conf. Num. Ship Hydro., UCB (1977).

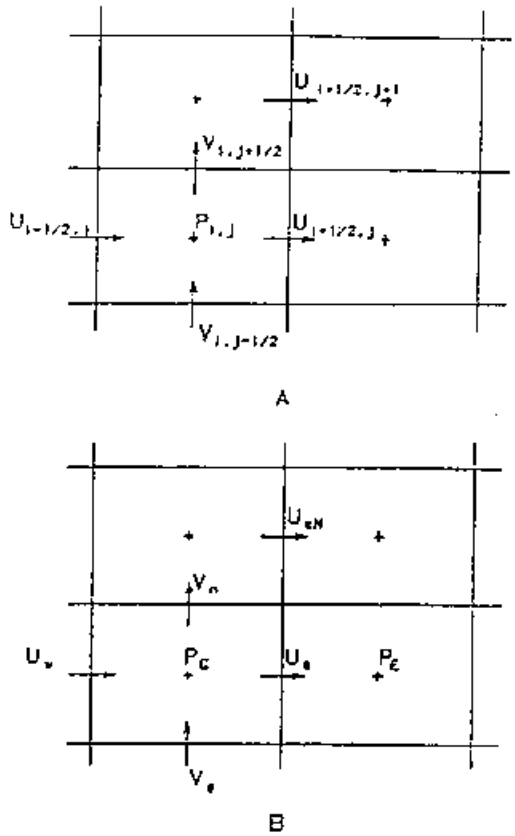

Fig. 1. Location of primary variables in mesh cell (A). Simplified notation used in text (B).

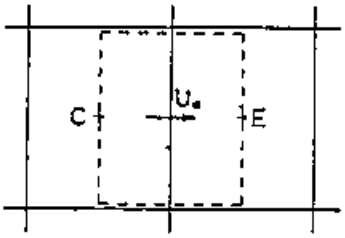

Fig. 2. Control volume (dashed line) for horizontal momentum equation.

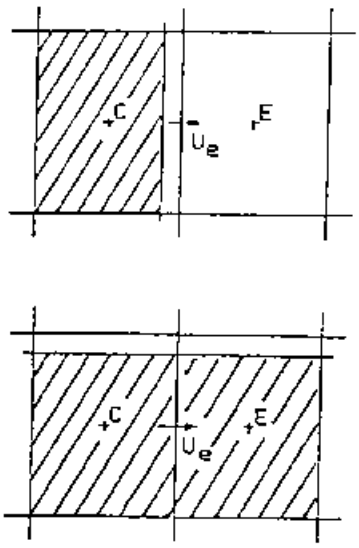

Fig. 3. Small cell volumes considered for worst-case stability estimates. Vertical interface (top) and horizontal interface (bottom).

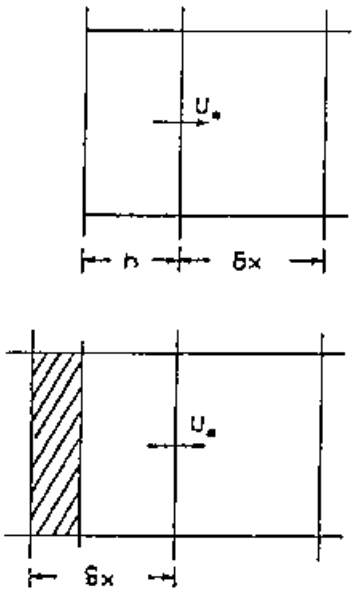

Fig. 4. Non-uniform mesh (top) compared with FAVOR method in uniform mesh (bottom).

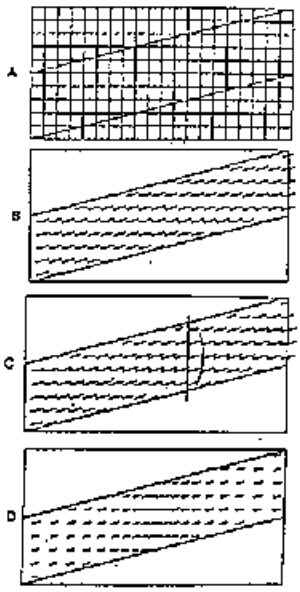

Fig. 5. Diagonal duct problem. (A) Duct orientation in mesh. (B) Initial uniform flow. (C) Calculated flow showing wall effect. (D) Calculated flow with wall boundary condition corrections.

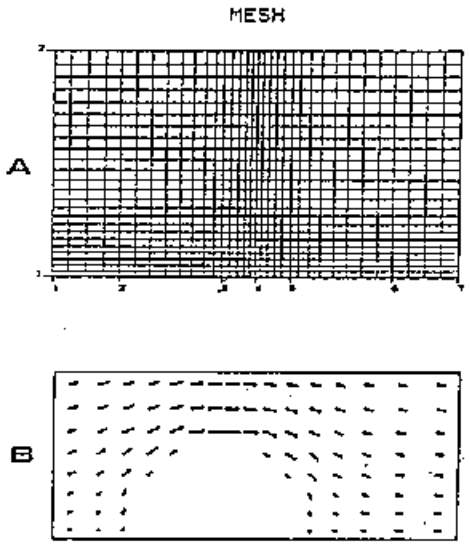

Fig. 6. Mesh used for flow about cylinder (A). Calculated potential flow in region near cylinder (B).

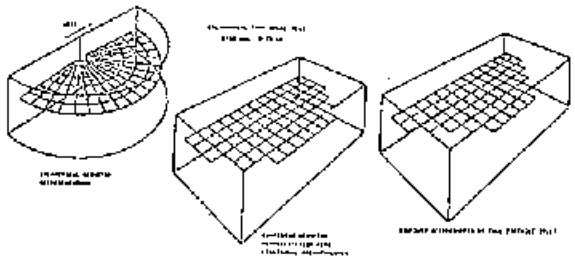

Fig. 7. Three models for cylindrical tank slosh. (A) Cylindrical coordinates. (B) FAVOR method in Cartesian coordinates. (C) Stepped boundary in Cartesian coordinates.

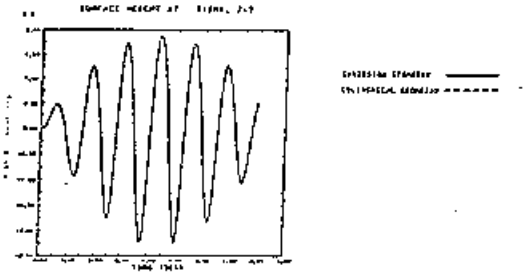

Fig. 8. Comparison of FAVOR method with cylindrical coordinate results for surface height versus time.

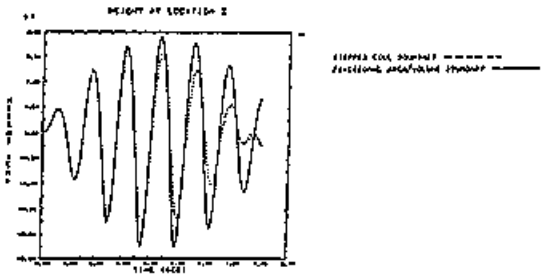

Fig. 9. Comparison of FAVOR method with stepped boundary results (dashed).

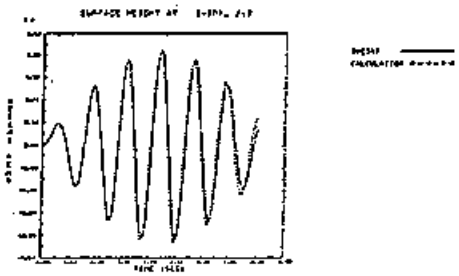

Fig. 10. Comparison of FAVOR method (dashed) with theory.

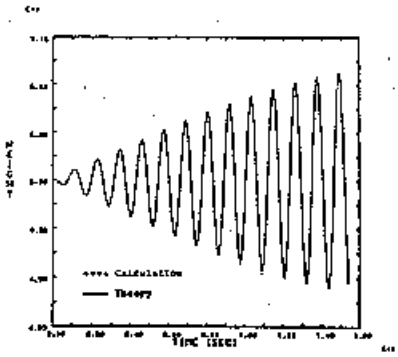

Fig. 11. Comparison of FAVOR calculations with theory for spherical tank slosh.

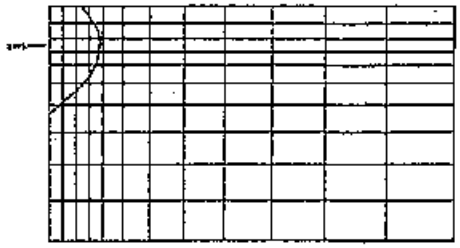

Fig. 12. Transverse mesh used for Wigley model calculation showing midship section.

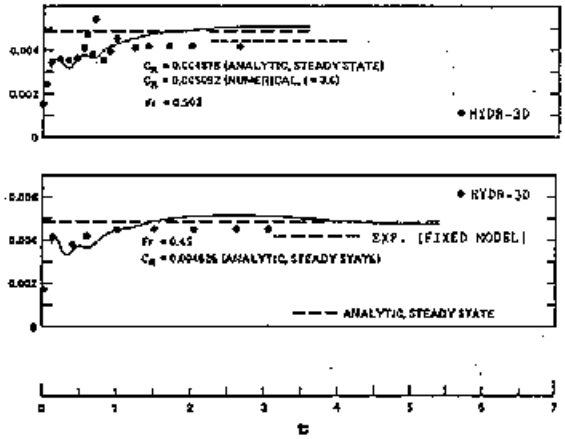

Fig. 13. Wave resistance versus time (in body lengths traversed) from Ref. 16. Froude number 0.503 top, 0.45 bottom.

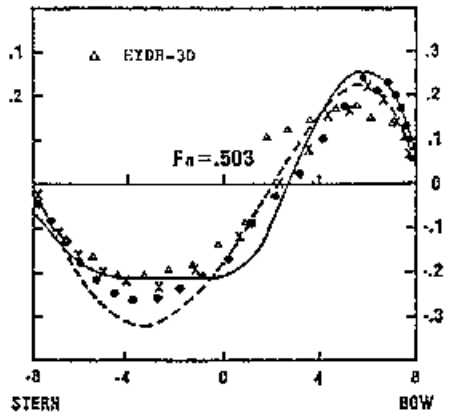

Fig. 14. Comparisons of computed wave profile with data from Ref. 15.